

# Sub-Kelvin Extension of the Theoretical Limit of MOSFET Subthreshold Swing

Arnout Beckers , Member, IEEE

**Abstract**—The theoretical limit of subthreshold swing in MOSFETs is extended down to sub-Kelvin temperatures. By including the band and band-tail states, the existence of a new phase 4 is derived from the theory. In phase 4, the subthreshold swing plateaus again when the Fermi level saturates inside the band. The model for subthreshold swing in phase 4 is proportional to a Fermi voltage instead of the thermal voltage. A short formula for the slope factor in phase 3 is also derived which allows to extract the subband density-of-states and effective mass. The phase-4 model allows to extract the Fermi level position. The proposed theoretical model is validated against experimental data from the recent literature. Even for a sharp band edge, the theory predicts that the subthreshold swing deviates from the Boltzmann thermal limit at sub-Kelvin temperatures.

**Index Terms**—Cryogenic, MOSFET, cryo-CMOS, device modeling, millikelvin, temperature, band tail

## I. INTRODUCTION

The subthreshold swing is defined as  $SS = (\partial V_{GS}/\partial \Psi_s) \cdot [\partial \Psi_s/\partial \log_{10}(I_{DS})]$ , which represents the required increment in gate-source voltage ( $V_{GS}$ ) to obtain a decade rise in drain-source current ( $I_{DS}$ ). (The factor  $m = \partial V_{GS}/\partial \Psi_s$  is the non-ideality factor, and  $\Psi_s$  is the surface potential.) It is a long-standing research question how low  $SS$  can theoretically be at low temperatures [1]. With the modern pursuit of quantum computers, this question has gained significant industrial and commercial relevance to understanding the limitations of CMOS power budget at millikelvin temperatures [2].

$SS$  is expected to follow the thermal limit  $m \cdot k_B T/q \cdot \ln(10)$  in phase 1 ( $k_B$  is Boltzmann's constant,  $T$  is temperature, and  $q$  is the electron charge), and then stay flat below a critical temperature ( $T_c \approx 50$  K) in phase 2, saturating to a plateau  $m \cdot k_B T_c/q \cdot \ln(10)$  due to a band tail [3]–[7]. However, Oka *et al.* reported experimental evidence that  $SS$  in a large nMOSFET can drop below the plateau-like region and decrease again in proportion to  $T$  in phase 3 (below  $\approx 1$  K) [8]. Their phase-3 discovery is promising for lowering the voltage in sub-Kelvin electronic circuits [9]–[11]. Recently, Yurttagül *et al.* have observed phase-3 behavior for  $T > 1$  K in silicon-on-insulator nMOS and pMOS devices [11]. However, their nMOS experiment, replotted in Fig. 1, shows a second plateau (phase 4), which has not been explained. Furthermore, the phase-3 model from Oka *et al.* in [Fig.13 in [8]], can be further

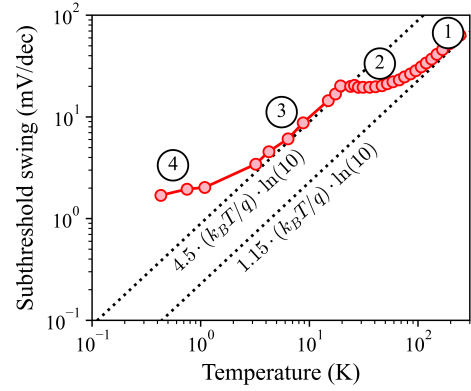


Fig. 1. Experimental data from Yurttagül *et al.* [11] measured in an undoped fully-depleted silicon-on-insulator nMOS device ( $W/L = 1$ ,  $V_{DS} = 25$  mV) fabricated in a custom CMOS pilot line with a poly-Si/SiO<sub>2</sub> gate stack. (1-2-3) are the 3 known  $T$ -phases and (4) is the new phase where a second plateau appears below phase 3.

brought into a short physical formula. Section II describes the framework which builds on the Gauss hypergeometric theory from [3], and properly includes the band states. Section III derives specific expressions for phases 3 and 4 of  $SS(T)$ , and Section IV compares these with the experiments from [8], [11].

## II. THEORETICAL FRAMEWORK

$SS(T)$  is usually extracted at a fixed  $I_{DS}$  in subthreshold at a low drain-source voltage ( $V_{DS}$ ). Assuming  $I_{DS}$  proportional to the mobile charge density,  $Q_m$ , we have

$$SS = \frac{\partial V_{GS}}{\partial \Psi_s} \cdot \frac{Q_m}{(\partial Q_m/\partial \Psi_s)} \cdot \ln(10). \quad (1)$$

From  $V_{GS} = \Psi_s + \Phi_{ms} + (Q_m + Q_d + Q_{it})/C_{ox}$  (where  $\Phi_{ms}$  is the metal-semiconductor work-function difference,  $Q_d$  is the depletion charge density,  $Q_{it}$  is the charge density trapped at the gate-oxide/channel interface, and  $C_{ox}$  is the gate-oxide capacitance), we obtain the derivative

$$\frac{\partial V_{GS}}{\partial \Psi_s} = m_0 + \frac{1}{C_{ox}} \cdot \left( \frac{\partial Q_m}{\partial \Psi_s} + \frac{\partial Q_{it}}{\partial \Psi_s} \right), \quad (2)$$

where  $m_0 = 1 + C_d/C_{ox}$  and  $C_d$  is the depletion capacitance. In the conventional theory of  $SS$  saturation the band tail is assumed to hold mobile states, contributing to  $Q_m$ , to obtain a completely flat plateau in phase 2 [3]–[5]. The phase-3 behavior in Fig. 1 was explained by considering the exponential band-tail states as immobile (“traps”) [8]. Therefore, Fig. 2 shows the density-of-states split into the band tail and the band

This work has received funding from the European Union's Horizon research and innovation programme under grant agreement number 101075725 ARCTIC.

A. Beckers is with imec, Kapeldreef 75, 3001 Leuven, Belgium.

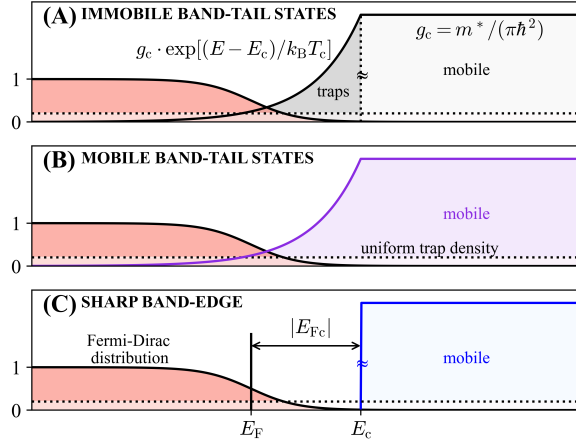


Fig. 2. Fermi-Dirac distribution, band tail, subband, and a uniform interface-trap density (dotted horizontal lines) are shown. (A) band tail with traps, (B) band tail with transport, and (C) no band tail.

for **three hypotheses**: (A) the band tail contributes traps, (B) the band tail contributes mobile states, and (C) no band tail. Each hypothesis has phases 1 to 4 depending on the Fermi level ( $E_F$ ) position with respect to the band edge ( $E_c$ ): (1)  $E_F \ll E_c$ , (2)  $E_F < E_c$ , (3)  $E_F \approx E_c$ , and (4)  $E_F > E_c$ .

For **hypothesis (A)**,  $Q_m = Q_{\text{band}}$  and  $Q_{\text{it}} = Q_{\text{it,u}} + Q_{\text{bt}}$ , where  $Q_{\text{band}} = q \cdot g_c \cdot k_B T \cdot \ln(1 + e^{q\Psi_s/k_B T})$  with  $g_c = m^*/(\pi\hbar^2)$ ,  $m^*$  is the effective mass, and  $q \cdot \Psi_s = E_{F_c} = E_F - E_c$ . Here  $Q_{\text{bt}}$  is given by a Gauss hypergeometric function,  $Q_{\text{bt}} = q \cdot g_c \cdot k_B T_c \cdot H_{2F1}(1, \theta, \theta + 1, z)$ , where  $\theta = T/T_c$  and  $z = -e^{-q\Psi_s/k_B T}$  [3]. The derivative is  $\partial Q_{\text{bt}}/\partial \Psi_s = q \cdot g_c \cdot k_B T_c \cdot \partial H_{2F1}/\partial z \cdot \partial z/\partial \Psi_s$ . Using a Gauss contiguous relation,  $\partial H_{2F1}/\partial z = (b/z) \cdot [H_{2F1}(a, b + 1, c, z) - H_{2F1}(a, b, c, z)]$  [12]; applying  $H_{2F1}(a, b, b, z) = (1 - z)^{-a}$  [12], and recognizing  $Q_{\text{bt}}$  and  $\partial Q_{\text{band}}/\partial \Psi_s = q^2 g_c / (1 + e^{-q\Psi_s/k_B T})$ , we find  $\partial Q_{\text{bt}}/\partial \Psi_s = q \cdot Q_{\text{bt}} / (k_B T_c) - \partial Q_{\text{band}}/\partial \Psi_s$ . Combining this expression with (1) and (2), gives

$$SS_{(A,1-4)} = \left( m_1 + \frac{q}{C_{\text{ox}}} \cdot \frac{Q_{\text{bt}}}{k_B T_c} \right) \cdot \xi \cdot \ln(10), \quad (3)$$

where  $\xi = k_B T / q \cdot \ln(1 + e^{E_{F_c}/k_B T}) \cdot (1 + e^{-E_{F_c}/k_B T})$ ,  $m_1 = 1 + (C_d + C_{\text{it,u}})/C_{\text{ox}}$  and  $C_{\text{it,u}} = \partial Q_{\text{it,u}}/\partial \Psi_s$ .

For **hypothesis (B)**,  $Q_m = Q_{\text{band}} + Q_{\text{bt}}$  and  $Q_{\text{it}} = Q_{\text{it,u}}$  in (1) and (2), thus it can be shown that

$$SS_{(B,1-4)} = \left( m_1 + \frac{q}{C_{\text{ox}}} \cdot \frac{Q_{\text{bt}}}{k_B T_c} \right) \cdot \frac{k_B T_c}{q} \cdot \left( 1 + \frac{Q_{\text{band}}}{Q_{\text{bt}}} \right) \cdot \ln(10). \quad (4)$$

Inspection of (4) indeed shows that  $SS_{(B,1-4)}$  does not drop below the plateau  $m_1 \cdot k_B T_c / q \cdot \ln(10)$  because  $Q_{\text{bt}} > 0$  and  $Q_{\text{band}} > 0$ . For **hypothesis (C)**,  $Q_m = Q_{\text{band}}$  and  $Q_{\text{it}} = Q_{\text{it,u}}$  in (1) and (2), thus it can be shown that

$$SS_{(C,1-4)} = \left( m_1 + \frac{1}{C_{\text{ox}}} \cdot \frac{q^2 g_c}{1 + e^{-E_{F_c}/k_B T}} \right) \cdot \xi \cdot \ln(10). \quad (5)$$

Fig.3 shows the three models (3–5) for the three different hypotheses in log-log scale. In phase 4,  $SS$  for hypotheses (A) and (C) saturates to a second plateau. For (B), the first plateau of [3] continues down to sub-Kelvin temperatures.

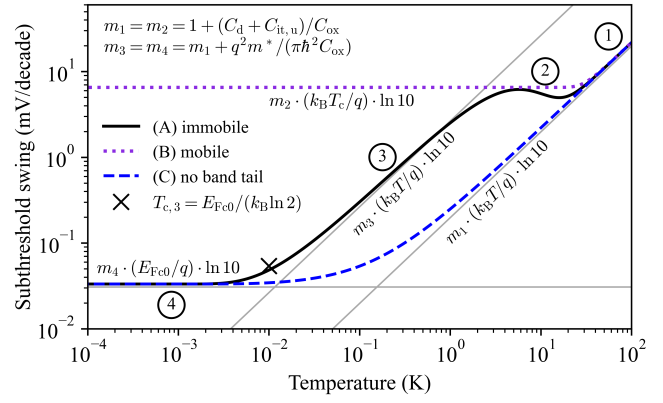


Fig. 3. Subthreshold swing models (3), (4), and (5) versus  $T$  in log-log scale. In phase 4,  $E_F$  is inside the subband (above  $E_c$ ) and the model transitions from being proportional to  $k_B T$  to  $E_{F_c}$  at  $T_{c,3} = 10$  mK.

### III. DERIVATION OF PHASE 3 AND PHASE 4 EXPRESSIONS

In the non-degenerate limit ( $E_{F_c} \ll 0$ ), (3) reduces to the expression given by Oka *et al.* in the inset of [Fig.13 in [8]],

$$SS_{(A,1-3)} = \left( m_1 + \frac{q}{C_{\text{ox}}} \cdot \frac{Q_{\text{bt}}}{k_B T_c} \right) \cdot \frac{k_B T}{q} \cdot \ln(10), \quad (6)$$

where  $C_{\text{bt}} = q \cdot Q_{\text{bt}}/k_B T_c$  is the band-tail capacitance. However, it should be highlighted that a concise formula can be derived for phase 3 which features fundamental constants. Taking the limit of  $SS_{(A,1-3)}$  as  $T \rightarrow 0$  and  $E_F \rightarrow E_c$  (i.e.,  $\Psi_s \rightarrow 0$ ), the total charge density in the band tail is  $Q_{\text{bt}} = q \cdot g_c \cdot k_B T_c$ , because the band-tail traps are filled if  $E_F$  reaches  $E_c$  and because  $\lim_{\theta \rightarrow 0} \lim_{\Psi_s \rightarrow 0} H_{2F1}(1, \theta, \theta + 1, -e^{-q\Psi_s/k_B T}) = H_{2F1}(1, 0, 1, -1) = 1$ , thus  $SS_{(A,3)}$  is

$$SS_{(A,3)} = m_3 \cdot \frac{k_B T}{q} \cdot \ln(10), \quad (7)$$

where  $m_3 = m_1 + q^2 g_c / C_{\text{ox}} = m_1 + q^2 m^*/(\pi\hbar^2 C_{\text{ox}})$ . Fig.3 shows that phase (A,3) is a thermal limit similar to phase 1, but multiplied with a higher slope factor ( $m_3 > m_1$ ) since the band tail provides significantly more traps than the uniform trap density. Expression (7) confirms Oka's observation that the essential parameter for the  $SS$  behavior in the millikelvin range is  $g_c$  ( $D_0$ ) rather than  $T_c$  ( $E_W$ ). The precise formulation (7) clearly shows this direct dependence on  $g_c$  instead of the integral in Oka's expression [8]. It also allows to extract the important physical parameters  $m^*$ ,  $g_c$  and/or  $C_{\text{ox}}$  from  $m_3$ .

In phase 4, by taking the limit of  $SS_{(A,1-4)}$  as  $\theta \rightarrow 0$  while  $E_F$  is above  $E_c$  ( $E_{F_c} > 0$ ), gives  $H_{2F1}(1, 0, 1, 0) = 1$  and  $\xi \approx E_{F_c}/q$ , thus  $SS_{(A)}$  in phase 4 is given by

$$SS_{(A,4)} = m_4 \cdot \frac{E_{F_c}}{q} \cdot \ln(10), \quad (8)$$

where  $m_4 = m_3$  and  $E_{F_c}/q$  is a Fermi voltage. If  $E_F > E_c$ ,  $SS$  becomes proportional to a Fermi voltage instead of a thermal voltage or band tail decay.  $SS$  in phase 4 is thus proportional to the distance  $E_{F_c} = E_F - E_c$ , which is positive in phase 4. Phase 4 comes out of (B) and (C) as well, when  $Q_{\text{band}} = q g_c E_{F_c} \gg Q_{\text{bt}} = q g_c k_B T_c$  in (4), and  $E_{F_c} > 0$

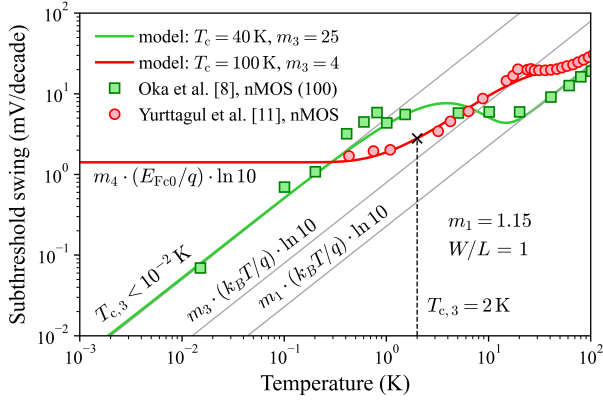


Fig. 4. For Yurttagül's data (red circular markers),  $T_{c,3}$  happens at 2 K, and there is a phase 4, while for Oka's data phase 4 is expected to arise at  $T < 10$  mK.  $T_{c,3}$  is the temperature at which  $E_F = E_c$ .

and  $\xi \approx E_{Fc}/q$  in (5). For (C),  $SS$  also deviates from the Boltzmann limit as shown with the dashed line in Fig.3.

#### IV. EXPERIMENTAL VALIDATION AND PHYSICAL PARAMETER EXTRACTION

Fig. 4 shows Oka's bulk nMOS (100) experiment (square markers) and Yurttagül's FDSOI nMOS experiment (circular markers). To plot (3) over all phases, an *ansatz* must be made for the behavior of  $E_{Fc}(T)$ . The temperature behavior of  $E_{Fc}$  saturates to  $E_{Fc0}$  in the 0-K limit. Focusing on (A) and (C), a good estimate for  $E_{Fc}(T)$  can be obtained from rewriting  $Q_{\text{band}}$  for  $E_{Fc}(T)$  and noting that  $Q_{\text{band}}$  in the 0-K limit is  $qg_c E_{Fc0}$  and that  $\lim_{x \rightarrow 0} x \ln(e^{c/x} - 1) = c$ , therefore we obtain the expression  $E_{Fc}(T) = k_B T \cdot \ln(e^{E_{Fc0}/k_B T} - 1)$ . The temperature at which  $E_{Fc}(T) = 0$  is  $T_{c,3} = E_{Fc0}/(k_B \ln 2)$ , which is the end of phase 3. For Yurttagül's data in Fig.4, we find that  $T_{c,3} = 2$  K and thus  $E_F$  is  $120 \mu\text{eV}$  above the band edge. For Oka's data, the  $E_F$  has not yet entered the subband at the reported temperatures in this particular device. From the phase-3 fit in Fig.4, we find that  $m_3 = 25$  for Oka's data and  $m_3 = 4$  for Yurttagül's data. From the  $m_3$  formula in (7) and Oka's reported  $t_{\text{ox}} = 6.8$  nm value for  $\text{SiO}_2/\text{poly-Si}$  gate stack ( $C_{\text{ox}} = 5$  mF m $^{-2}$ ), it is possible to extract the subband density of states ( $g_c = 7.4 \times 10^{13}$  cm $^{-2}$  eV $^{-1}$ ) and the effective mass at millikelvin temperatures ( $m^* = 0.18 \cdot m_e$ ).

#### V. CONCLUSION

The theoretical limit of subthreshold swing in MOSFETs is investigated down to sub-K temperatures for three hypotheses about the band tail (traps, transport, none). For each hypothesis, the theory predicts a proportionality to  $E_{Fc}(T)/q \cdot \ln(10)$  if the Fermi level lies inside the subband (phase 4). If the Fermi level also saturates inside the subband, the model predicts a plateau in phase 4, which was successfully tested against the first measurement of a phase 4 in the literature. For phase 3 with immobile band-tail states, a slope factor expression was derived,  $m_3 = m_1 + q^2 m^*/(\pi \hbar^2 C_{\text{ox}})$ , which allows to extract  $m^*$  or  $C_{\text{ox}}$  from phase-3 measurements. In the hypothetical case of a perfectly sharp band edge, phase 4 does not follow the Boltzmann thermal limit at sub-Kelvin temperatures.

#### REFERENCES

- [1] S. Tewksbury, "Attojoule MOSFET logic devices using low voltage swings and low temperature," *Solid-State Electronics*, vol. 28, pp. 255–276, Mar. 1985. doi: 10.1016/0038-1101(85)90006-1.
- [2] M. Gonzalez-Zalba, S. De Franceschi, E. Charbon, T. Meunier, M. Vinet, and A. Dzurak, "Scaling silicon-based quantum computing using CMOS technology," *Nature Electronics*, vol. 4, no. 12, pp. 872–884, 2021. doi: 10.1038/s41928-021-00681-y.
- [3] A. Beckers, F. Jazaeri, and C.ENZ, "Theoretical Limit of Low Temperature Subthreshold Swing in Field-Effect Transistors," *IEEE Electron Device Letters*, vol. 41, pp. 276–279, Feb. 2020. doi: 10.1109/LED.2019.2963379.
- [4] H. Bohuslavskyi, A. G. M. Jansen, S. Barraud, V. Barral, M. Cassé, L. Le Guevel, X. Jehl, L. Hutin, B. Bertrand, G. Billiot, G. Pillonnet, F. Arnaud, P. Galy, S. De Franceschi, M. Vinet, and M. Sanquer, "Cryogenic Subthreshold Swing Saturation in FD-SOI MOSFETs Described With Band Broadening," *IEEE Electron Device Letters*, vol. 40, pp. 784–787, May 2019. doi: 10.1109/LED.2019.2903111.
- [5] G. Ghibaudo, M. Aouad, M. Cassé, S. Martinic, T. Poiroux, and F. Balestra, "On the modelling of temperature dependence of subthreshold swing in MOSFETs down to cryogenic temperature," *Solid-State Electronics*, vol. 170, p. 107820, Aug. 2020. doi: 10.1016/j.sse.2020.107820.
- [6] I. M. Hafez, G. Ghibaudo, and F. Balestra, "Assessment of interface state density in silicon metal-oxide-semiconductor transistors at room, liquid-nitrogen, and liquid-helium temperatures," *Journal of Applied Physics*, vol. 67, pp. 1950–1952, Feb. 1990. doi: 10.1063/1.345572.
- [7] R. M. Jock, S. Shankar, A. M. Tyryshkin, J. He, K. Eng, K. D. Childs, L. A. Tracy, M. P. Lilly, M. S. Carroll, and S. A. Lyon, "Probing band-tail states in silicon metal-oxide-semiconductor heterostructures with electron spin resonance," *Applied Physics Letters*, vol. 100, p. 023503, Jan. 2012. doi: 10.1063/1.3675862.
- [8] H. Oka, H. Asai, T. Inaba, S. Shitakata, H. Yui, H. Fuketa, S. Iizuka, K. Kato, T. Nakayama, and T. Mori, "Milli-Kelvin Analysis Revealing the Role of Band-edge States in Cryogenic MOSFETs," in *2023 International Electron Devices Meeting (IEDM)*, (San Francisco, CA, USA), pp. 1–4, IEEE, Dec. 2023. doi: 10.1109/IEDM45741.2023.10413872.
- [9] R. Acharya, S. Brebels, A. Grill, J. Verjauw, T. Ivanov, D. P. Lozano, D. Wan, J. Van Damme, A. Vadiraj, M. Mongillo, *et al.*, "Multiplexed superconducting qubit control at millikelvin temperatures with a low-power cryo-CMOS multiplexer," *Nature Electronics*, vol. 6, no. 11, pp. 900–909, 2023. doi: 10.1038/s41928-023-01033-8.
- [10] L. Le Guevel, G. Billiot, B. Cardoso Paz, M. L. V. Tagliaferri, S. De Franceschi, R. Maurand, M. Cassé, M. Zurita, M. Sanquer, M. Vinet, X. Jehl, A. G. M. Jansen, and G. Pillonnet, "Low-power transimpedance amplifier for cryogenic integration with quantum devices," *Applied Physics Reviews*, vol. 7, p. 041407, 12 2020. doi: 10.1063/5.0007119.
- [11] N. Yurttagül, M. Kainlauri, J. Toivonen, S. Khadka, A. Kannianen, A. Kumar, D. Subero, J. Muhonen, M. Prunnila, and J. S. Lehtinen, "Millikelvin Si-MOSFETs for Quantum Electronics," Oct. 2024. arXiv:2410.01077 [cond-mat, physics:physics].
- [12] I. S. Gradshtēin and D. Zwillinger, *Table of integrals, series, and products*, 8th edition. Elsevier Academic Press, 2015.